NASA CONTRACTOR REPORT

NASA CR-2898

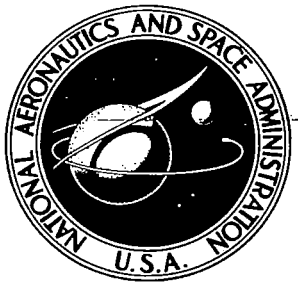

NASA CR-2

UNSTEADY SUPERSONIC AERODYNAMIC THEORY FOR INTERFERING SURFACES BY THE METHOD OF POTENTIAL GRADIENT

William P. Jones and Kari Appa

Prepared by
BELL AEROSPACE TEXTRON
Buffalo, N.Y. 14240
for Langley Research Center

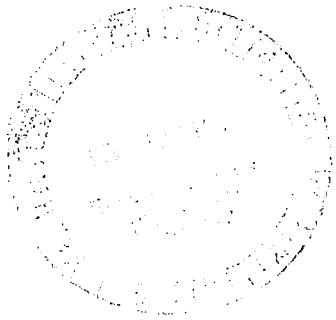

NATIONAL AERONAUTICS AND SPACE ADMINISTRATION • WASHINGTON, D. C. • OCTOBER 1977

1. Report No.	2. Government Accession No.	3. Recipient's Catalog No.
NASA CR-2898		

4. Title and Subtitle	5. Report Date
Unsteady Supersonic Aerodynamic Theory for Interfering Surfaces By The Method of Potential Gradient	October 1977
	6. Performing Organization Code
7. Author(s)	8. Performing Organization Report No.
William P. Jones and Kari Appa	
9. Performing Organization Name and Address	10. Work Unit No.
Bell Aerospace Textron Buffalo, New York 14240	11. Contract or Grant No. NAS1-13986
	13. Type of Report and Period Covered
12. Sponsoring Agency Name and Address	Contractor Report
National Aeronautics and Space Administration Washington, D.C. 20546	14. Sponsoring Agency Code

15. Supplementary Notes

Langley Technical Monitor: Robert W. Hess
Final Report

16. Abstract

A generalized solution of the hyperbolic wave equation, derived by W.P. Jones, has been further developed to relate the velocity components at a field point to the potential gradient distribution in the dependence domain. Singular integrals have been evaluated in closed form, with numerical integration methods for more complex but analytic functions. Idealization of the lifting surfaces by trapezoidal elements with two sides parallel to the streamlines is computationally efficient. Streamwise integrals are performed analytically, and spanwise integrals are necessary only on element leading and trailing sides. Furthermore, all integrands vanish on the Mach cone and the need for determining the hyperbolic curves of intersection of the cone with the lifting surface is avoided. The elements are also advantageous for automatic grid generation which has been incorporated in associated computer manuals.

Pressure distribution on a double delta wing and generalized aerodynamic coefficients for three AGARD planforms have been calculated and compared with the available results.

17. Key Words (Selected by Author(s))	18. Distribution Statement
Supersonic, Unsteady, Aerodynamics, Interfering, Potential Gradient,	Unclassified - Unlimited Subject Category 02

19. Security Classif. (of this report)	20. Security Classif. (of this page)	21. No. of Pages	22. Price*
Unclassified	Unclassified	38	$4.00

*For sale by the National Technical Information Service, Springfield, Virginia 22161.

CONTENTS

LIST OF TABLES

LIST OF ILLUSTRATIONS

UNSTEADY SUPERSONIC AERODYNAMIC THEORY FOR INTERFERING SURFACES BY THE METHOD OF POTENTIAL GRADIENT

by

William P. Jones
Aerospace Engineering
Texas A&M University, Texas

and

Kari Appa
Niagara Frontier Operations
Bell Aerospace Textron
Buffalo, New York 14240

SYMBOLS

k,k'	Reduced frequencies, $\frac{\omega \ell}{U}$, $\frac{kM}{\beta}$
$2\pi K$	Modified potential difference across the lifting surface
ℓ	Reference length
$\hat{\ell},\hat{m},\hat{n}$	Direction cosines of a normal to the lifting surface
$\tilde{\ell}$	Local lift
m	Slope of a line
M	Mach number
n	Unit normal or summation variable
q	$\frac{1}{2}\rho U^2$ dynamic pressure
Q_{ij}	Generalized aerodynamic coefficients $= \frac{Q_{ij}}{q\ell^3}$
S	Surface of integration
R^2	Hyperbolic radius squared $(X_o-X)^2 - (Y_o-Y)^2 - (Z_o-Z)^2$
t	Dimensional time
T	Nondimensional time, $\frac{Ut}{\ell}$
U	Air stream velocity
U_{2n},V_{2n},W_{2n}	Induced velocity components, also termed as backwash, sidewash and normalwash components

W	Influence coefficient matrix relating normal velocity and velocity doublets
x,y,z	Dimensional space coordinates
X,Y,Z	Nondimensional space coordinates, $\frac{x}{\ell\beta}, \frac{y}{\ell}, \frac{z}{\ell}$
$\overline{X}$	A transformation matrix, Eq. 48.
α	Constant of a line
β	$= \sqrt{M^2 - 1}$
η_D	Displacement normal to the lifting surface $\equiv \ell\tilde{\eta} \exp(ikT)$
η	$= Y_o - Y$
ξ	$= X_o - X$
ρ	Air density
ϕe^{ikT}	Velocity potential, a scalar quantity
Φ	$= \phi e^{ik'Mx}$ Modified potential
ω	Circular frequency of harmonic motion, radians per second

INTRODUCTION

Accurate determination of unsteady aerodynamic forces is essential for precise evaluation of the aeroelastic stability characteristics of flight vehicles. In the subsonic case, the integral formulation is simple and computational methods have been well developed (ref. 2). In the supersonic case, the problem is complicated by the fact that pressure discontinuities arise because of the conical flow field emanating from geometric irregularities such as cranked leading edges, wing tips and interfering/interacting surfaces. A closed form solution for such problems is unlikely, and numerical superposition methods of finite element type, using sources, velocity potential doublets or pressure doublets as basic variables have received attention in the literature (refs. 3-24).

The source superposition method gives a very simple integral relationship between the potential and the downwash field (which is determined by the mode shapes) in the non-interacting case (ref. 3). However, in the interacting case, the potential is first related to the source strength and this is in turn related to the downwash distribution (ref. 4). Thus, by this method, two sets of equations are involved in solving the problem. In addition, integration over wake regions and non-unique "diaphragms" is necessary as a part of the solution.

In the velocity potential method, there is a direct relationship between the downwash (the mode shapes) and the velocity potential (ref. 1). Diaphragm regions are no longer necessary and the wake regions do not need detailed modeling since their behavior is determined by the trailing edge potentials of the wake-producing surface. The integral relations which are more complicated than in the source superposition method have been considerably simplified in the current work.

The pressure potential or kernel function method is a 'direct' approach via a relation between downwash and pressures and aerodynamic coefficients (refs. 5-8). This integral relation is, however, even more complicated than in the velocity potential approach.

For arbitrary configurations, the numerical methods employed may broadly be classified as collocation and finite element methods. Collocation methods assume, a priori, certain mode shapes or series expansions of the unknown parameters such as pressure and doublet strengths. The coefficients of these series or modes are determined from a set of algebraic equations established by satisfying the integral relation only at an appropriate number of collocation points. The number of equations is comparatively few and is computationally efficient for simple configurations (ref. 9). In a recent paper, Cunningham (ref. 10) uses the three-dimensional kernel function with a judicious selection of pressure functions for interacting surface configurations. However, the application of pressure collocation methods to handle general configurations is complicated by the difficulty of choosing pressure modes for complex multi-dimensional shapes such as wing-body combinations.

In finite element methods, the integration over the dependence domain is replaced by a sum of integrations over a number of simple elemental domains (finite elements). Over each area element, the unknown parameter is expressed as a sum of simple functions. A number of finite element shapes have been used, such as squares, Mach or characteristic boxes, and triangular or quadrilateral elements. Numerical approaches differ also in the choice of functional variation within each element and in the integration method over the element (refs. 11-20).

In Mach or characteristic box schemes, planform edges have usually been approximated by jagged representations which result in erratic behavior of the pressure over the whole surface. More recent versions of Mach box programs are described in references 11 and 12.

Stark (ref. 13) used elementary characteristic boxes in developing a digital computer program in which special consideration was given to the handling of subsonic singular leading edges. These modifications, however, detract very significantly from the basic simplicity of the Mach or characteristic box approach, the computational price paid for additional accuracy being large.

A triangular representation of the dependence domain using a linear distribution of sources was developed in references 14 and 15. This method offers acceptable accuracies with far fewer elements than other methods.

Allen and Sadler (ref. 17), using characteristic elements, developed a doublet superposition method based on Jones' integrated potential formulation for planar configurations. They expressed the kernel (sine and cosine) functions as parabolic interpolation functions within each element. Woodcock and York (ref. 18) extended this approach to interacting wing and wing-body configurations.

The integrated potential approach was further developed in reference 23, using linearly varying potential doublets within triangular elements. Closed form integrals were employed to evaluate the singular functions, while numerical integration methods were adopted for more complex but analytic functions.

Although good results were obtained with fewer elements, an arbitrary wing with a control surface could not satisfactorily be idealized. This disadvantage of the velocity potential method led to the development of the potential gradient method described in reference 25 and this report. In this scheme, the potential gradient in the stream direction is considered as an independent variable and is assumed to be constant over an element. This results in fewer integrals than in the velocity

potential method discussed in reference 23. Once again closed form integrals have been obtained for singular functions and recurrence formulae derived for non-singular terms. Two sides of a typical quadrilateral element are taken parallel to the stream, and computational efficiency is increased because the integrals along these two lines and along the boundary of the area of the wing cut by the Mach cone vanish. This type of element has also facilitated the provision of automatic grid generation. Velocity potential distributions and generalized aerodynamic coefficients have been obtained by the use of the potential gradient method and compared with available results derived by other methods.

GENERAL AERODYNAMIC ANALYSIS

In the present analysis the coordinates x, y, z and time t are replaced in nondimensional form by X, Y, Z and T, respectively, where

$$X = \frac{x}{\ell\beta}\ ,\quad Y = \frac{y}{\ell}\ ,\quad Z = \frac{z}{\ell}\ ,\quad T = \frac{Ut}{\ell} \tag{1}$$

ℓ being the standard length, U the airspeed, and $\beta = [M^2 - 1]^{1/2}$ where M is the Mach number. The effect of the above transformation is to change the planform of the wing in such a way that its chord is lengthened while its lateral dimensions remain the same. At the same time the Mach lines in the X, Y, Z coordinate system are inclined at $\pm 45°$ to the X axis as indicated in Figure 1.

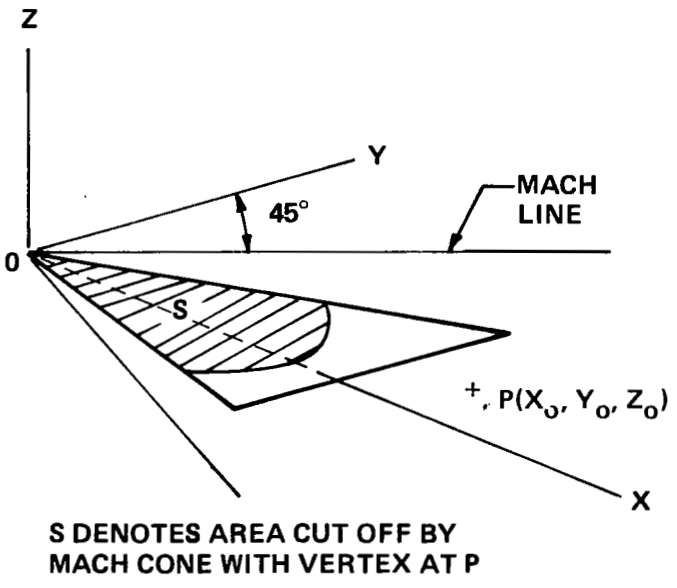

Figure 1. Domain of Influence in Supersonic Flow

Next let us suppose that a delta wing with subsonic leading edges is oscillating in the airstream with frequency ω rads/sec. Then if ϕe^{ikT}, the velocity potential of the disturbed flow, is replaced by a nondimensional modified potential Φ such that

$$\Phi = \frac{\phi}{U\ell} e^{ikM^2 X/\beta} , \tag{2}$$

it can be proved (ref. 1), that

$$\frac{\partial^2 \Phi}{\partial X^2} - \frac{\partial^2 \Phi}{\partial Y^2} - \frac{\partial^2 \Phi}{\partial Z^2} + k'^2 \Phi = 0, \tag{3}$$

where $k' = \frac{kM}{\beta}$ and $k = \frac{\omega \ell}{U}$. Furthermore, it is shown in reference 1 that the solution of Equation (3) may be expressed as the integral relation

$$\Phi (X_o, Y_o, Z_o) = - \frac{\partial}{\partial Z_o} \iint K (X, Y) \frac{\cos k'R}{R} dXdY \tag{4}$$

where the integral is taken over the part of the wing cut off by the Mach cone with vertex at X_o, Y_o, Z_o. The symbol $K \equiv (\Phi_a - \Phi_b)/2\pi$ denotes the difference between the modified velocity potential above and below the wing and

$$R = \left[(X_o - X)^2 - (Y_o - Y)^2 - (Z_o - Z)^2 \right]^{1/2} \tag{5}$$

The surface of the Mach cone with vertex at X_o, Y_o, Z_o is defined by $R = 0$ and the mean position of the wing is assumed to be in the plane $Z = 0$.

In general, the modes of motion of the wing are assumed to be known. The displacement normal to the wing's surface will be denoted by η_D [$\equiv \ell \tilde{\eta} \exp (ikT)$] where $\tilde{\eta}$ is a function of x and y. The condition for tangential flow over the wing may then be expressed as

$$\frac{d\eta_D}{dt} = \frac{\partial \phi}{\partial n} e^{ikT}$$

or

$$\frac{d\tilde{\eta}}{dT} = \left[\frac{\hat{\ell}}{\beta} \frac{\partial}{\partial X_o} + \hat{m} \frac{\partial}{\partial Y_o} + \hat{n} \frac{\partial}{\partial Z_o} \right] \Phi e^{-ik'M X} \tag{6}$$

where

$$\frac{d\tilde{\eta}}{dT} = ik\tilde{\eta} + \frac{1}{\beta} \frac{\partial \tilde{\eta}}{\partial X}$$

and $\frac{\partial \phi}{\partial n}$ is the velocity normal to the surface induced by the doublet distribution over the wing and the wake. The factor exp (ikT) is cancelled through Equation (2) and subsequently.

When the wing lies approximately in the plane $Z = 0$ and the displacement η_D is small, the above relation simplifies. In terms of the modified potential Φ and the nondimensional coordinates defined by Equation (1), the boundary condition to be satisfied at a typical point X_o, Y_o, Z_o is then obtained by differentiating Equation (4). For the case considered, Equation (6) is replaced by

$$\frac{\partial \Phi}{\partial Z_o} = \left[i k \tilde{\eta} + \frac{1}{\beta} \frac{\partial \tilde{\eta}}{\partial X_o} \right] e^{i k' M X_o} \tag{7}$$

$$= - \frac{\partial^2}{\partial Z_o^2} \iint K(X, Y) \frac{\cos k'R}{R} dX dY$$

When the appropriate K distribution that satisfies the above equation has been determined, the values of $\frac{\partial \Phi}{\partial X_o}$ and $\frac{\partial \Phi}{\partial Y_o}$ can be deduced from Equation (4) by differentiation. The actual velocity components $\frac{\partial \phi}{\partial X_o}, \frac{\partial \phi}{\partial Y_o}$ may then be derived by differentiating Equation (2).

The Modified Upwash

In order to determine the modified velocity components, it is convenient to express cos k'R in series form

$$\frac{\cos k'R}{R} = \sum_{n=o}^{N} C_{2n} R^{2n-1} \tag{8}$$

where

$$C_{2n} = \frac{(-1)^n k'^{2n}}{2n!} \tag{9}$$

The modified upwash W is then given by

$$W = \frac{\partial \Phi}{\partial Z_o} = \sum C_{2n} W_{2n} \tag{10}$$

where

$$W_{2n} = - \frac{\partial^2}{\partial Z_o^2} \iint K(X, Y) R^{2n-1} dX dY \tag{11}$$

and n = 0, 1, 2, etc.

When n = 0 and Z = 0,

$$W_o = - \frac{\partial^2}{\partial Z_o^2} \iint \frac{K}{R} d\xi \, d\eta \tag{12}$$

where $\xi = X_o - X$ and $\eta = Y_o - Y$. By integrating by parts, it may be deduced that

$$W_o = \frac{\partial^2}{\partial Z_o^2} \iint_S \frac{\partial K}{\partial \xi} \, L \, d\xi \, d\eta \tag{13}$$

where

$$L = \frac{1}{2} \log_e \left(\frac{\xi + R}{\xi - R} \right) \tag{14}$$

Let us next assume that the area of integration S is divided into a number of small quadrilateral elements E with chordwise sides parallel to the ξ or X axis. It is further supposed that $\frac{\partial K}{\partial \xi} \left(= - \frac{\partial K}{\partial X}\right)$ is constant over each element. Then, since $L = 0$ over the part of the boundary of S on the surface of the cone $R = 0$, it can be deduced that W_o is given approximately by

$$W_o = \sum_E \frac{\partial K}{\partial X} \frac{\partial}{\partial Z_o} \iint_S \frac{Z_o}{\eta^2 + Z_o^2} \left(\frac{\xi}{R}\right) d\xi \, d\eta \tag{15}$$

the sum of the contributions from all the E elements. The above equation, after integration with respect to ξ then yields

$$W_o = \sum_E \frac{\partial K}{\partial X} \oint \frac{\partial}{\partial Z_o} \left(\frac{Z_o R}{\eta^2 + Z_o^2} \right) d\eta \tag{16}$$

where $\oint$ denotes the contour integral around a quadrilateral element in the anti-clockwise direction as indicated in Figure 2. In Equation (16), ξ is replaced by $m\eta + \alpha$ where m and α have the values corresponding to the particular side of the quadrilateral over which the integration is being performed and

$$R = \left[(m^2 - 1)\eta^2 + 2m\alpha\eta + \alpha^2 - Z_o^2 \right]^{1/2} \tag{17}$$

It should be noted that $m^2 - 1$ can be negative and that $\alpha^2 \geq Z_o^2$. When the above expression for R is substituted in Equation (16), it can be shown that

$$W_o = - \sum_E \frac{\partial K}{\partial X} I_o \tag{18}$$

where I_o is given by

$$I_o = \left[\frac{R\eta}{\eta^2 + Z_o^2} - (m^2 - 1) F_o + m^2 Z_o^2 F_1 - m\alpha F_2 \right]_C \tag{19}$$

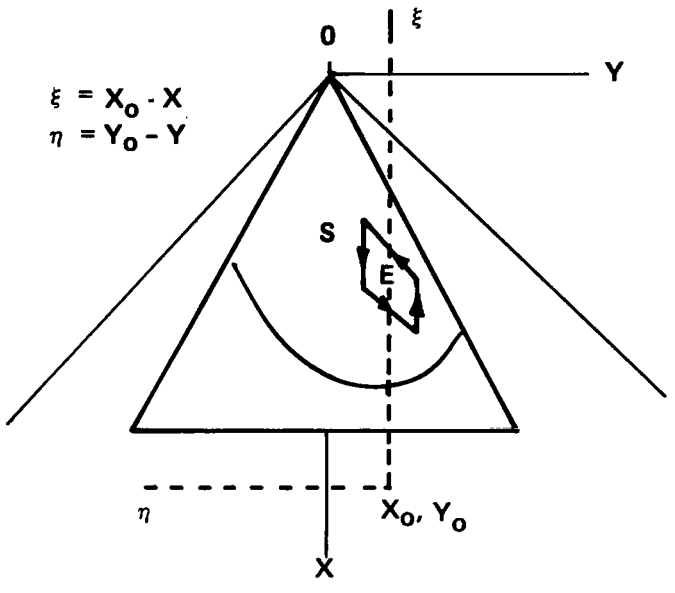

Figure 2. Contour Integration Along Discrete Elements

where

$$F_o = \oint \frac{d\eta}{R}$$

$$F_1 = \oint \frac{d\eta}{(\eta^2 + Z_o^2)R} \qquad (20)$$

$$F_2 = \oint \frac{\eta d\eta}{(\eta^2 + Z_o^2)R}$$

and $]_c$ indicates $\oint$ around each element E, Figure 2.

Since

$$\frac{dL}{d\eta} = \frac{mZ_o^2 - \eta\alpha}{(\eta^2 + Z_o^2)R} \qquad (21)$$

it follows that the value of F_2 can be derived from the relation

$$\alpha F_2 = mZ_o^2 F_1 - L \qquad (22)$$

Hence, only F_o and F_1 need be evaluated. It can readily be deduced that

$$F_o = \frac{1}{(m^2-1)^{1/2}} \log_e \frac{(m^2-1)^{1/2} R + (m^2-1)\eta + m\alpha}{m^2-1}, \quad \ldots m > 1$$

$$= \frac{1}{(1-m^2)^{1/2}} \sin^{-1} \frac{(1-m^2)\eta - m\alpha}{[\alpha^2 - Z_o^2(1-m^2)]^{1/2}} \quad \ldots . m < 1 \qquad (23)$$

$$= \frac{R}{\alpha} \quad \ldots . m = 1$$

The integral F_1 can also be derived by substituting $\eta = Z_o \tan(\theta+\gamma)$ in the integrand and putting $\tan\gamma = mZ_o/\alpha$. After some reduction, the required formula can be shown to be

$$F_1 = \frac{1}{Z_o(\alpha^2+m^2 Z_o^2)} \left[\alpha \sin^{-1} \left\{ \frac{\eta\alpha - mZ_o^2}{\left[(\eta^2+Z_o^2)\,[\alpha^2+Z_o^2(m^2-1]\right]} \right\}^{1/2} \right.$$

$$\left. + \frac{mZ_o}{2} \log_e \frac{(\xi+R)}{(\xi-R)} \right]_{\eta_1}^{\eta_2} \qquad (24)$$

where the integral is taken along the line $\xi = m\eta + \alpha$ from η_1 to η_2. It should be noted that the values of m and α are different for the lower side of the quadrilateral element.

When the values of all the F integrals over the upper and lower sides of each element have been determined, the total integral I_o for any element can be evaluated. From Equation (18), the upwash due to all the elements may then be obtained by summation.

Similarly, it can be deduced that

$$W_2 = \frac{\partial}{\partial Z} \iint \frac{KZ_o d\xi}{R} d\eta$$

$$= \sum_E \frac{\partial K}{\partial X} \oint \left(\xi L - R - \frac{Z_o^2 R}{\eta^2+Z_o^2} \right) d\eta \qquad (25)$$

$$= \sum_E \frac{\partial K}{\partial X} I_2(\eta)$$

where

$$I_2(\eta) = \left[\frac{\eta L(m\eta+2\alpha)}{2} - \frac{R\eta}{2} + \frac{F_o}{2}[\alpha^2 - 3(m^2-1)Z_o^2] \right.$$

$$\left. + \frac{Z_o^2 F_1}{2}(3mZ_o^2 - 4\alpha^2) - \frac{7m\alpha Z_o^2 F_2}{2} \right]_C \qquad (26)$$

is taken around the contour C of each element of area (Figure 2). The corresponding formula for W_{2n}, for $n \geq 2$ is given by

$$W_{2n} = (2n-1) \sum_{E} \frac{\partial K}{\partial X} I_{2n} \tag{27}$$

where

$$I_{2n} = \oint (H_{2n-2} - (2n-3) Z_o^2 H_{2n-4}) \, d\eta \tag{28}$$

in which

$$H_{2n} = \frac{R^{2n+1}}{2n(2n+1)} - \frac{(2n-1)}{2n} (\eta^2 + Z_o^2) H_{2n-2} \tag{29}$$

with

$$H_o = \xi L - R \tag{30}$$

and

$$H_2 = \frac{R^3}{6} - \frac{(\eta^2 + Z_o^2) H_o}{2} \tag{31}$$

The integrand in I_{2n} is analytic throughout the dependence domain and closed form integration is possible. However, it is more economical to evaluate the integral numerically, say, by the method of Gaussian quadrature. It is clear from the expressions for H_{2n} that the integrals I_{2n} vanish on the Mach boundary R = 0. This eliminates the need for the determination of the intersection of the dependent domain by the Mach hyperbola. However, for hyperbolic radius $R >> 1$ and n large, the magnitudes H_{2n} grow in geometric progression. The convergence of W for large values of reduced frequency k is then slow. However, for practical values of k and R convergence is obtained with a reasonable number of terms.

The Modified Backwash and Sidewash Components

The corresponding velocity components U_{2n}, V_{2n} along the OX and OY axes, respectively, may also be deduced.

It can readily be proved that

$$\frac{\partial \Phi_o}{\partial X_o} = U_o = Z_o \sum_{E} \frac{\partial K}{\partial X} (mF_2 + \alpha F_1) \tag{32}$$

$$\frac{\partial \Phi_2}{\partial X_o} = U_2 = Z_o \sum_{E} \frac{\partial K}{\partial X} (\eta L - mZ_o^2 F_2 - \alpha Z_o^2 F_1 + \alpha F_o) \tag{33}$$

and

$$\frac{\partial \Phi_{2n}}{\partial X_o} = U_{2n} = (2n-1) Z_o \sum_{E} \frac{\partial K}{\partial X} \oint P_{2n-2} \, d\eta \ldots\ldots n \geq 2 \tag{34}$$

where P_{2n} is defined by

$$P_{2n} = \int R^{2n-1}\, d\xi$$

$$= \frac{\xi R^{2n-1} - (2n-1)(\eta^2 + Z_o^2) P_{2n-2}}{2n} \tag{35}$$

with

$$P_o = L \tag{36}$$

and

$$P_2 = \frac{\xi R - (\eta^2 + Z_o^2) L}{2} \tag{37}$$

Similarly, the sidewash components are given by

$$\frac{\partial \Phi_o}{\partial Y_o} = V_o = + Z_o \sum_E \frac{\partial K}{\partial X} \left(\frac{R}{\eta^2 + Z_o^2} \right) \tag{38}$$

$$\frac{\partial \Phi_2}{\partial Y_o} = V_2 = + Z_o \sum_E \frac{\partial K}{\partial X} [(m\eta + \alpha) L - R] \tag{39}$$

and

$$\frac{\partial \Phi_{2n}}{\partial Y_o} = V_{2n} = + (2n-1) Z_o \sum_E \frac{\partial K}{\partial X} H_{2n-2} \ldots n \geqslant 2 \tag{40}$$

The Wake Field

In the wake, since it can sustain no lift,

$$\frac{\partial K}{\partial X} - \frac{ikK}{\beta} = 0 \tag{41}$$

This implies that

$$K(X) = K(X_{TE})\, e^{\frac{ik}{\beta}(X - X_{TE})} \tag{42}$$

where $K(X_{TE})$ is the value of K at the trailing edge of the wing section being considered. If the wake is assumed to lie in the plane Z = 0, its contribution to the normal modified velocity component can readily be deduced since

$$\frac{\partial K}{\partial X} = \frac{i\ k\ K(X_{TE})}{\beta} e^{\frac{i k}{\beta}(X-X_{TE})} \tag{43}$$

and $K(X_{TE})$ is the sum of the $\frac{\partial K}{\partial X}$ values for all the elements upstream. Using the $\frac{\partial K}{\partial X}$ distribution given by Equation (43), the contribution to the velocity components at a receiving element from the wake elements can be written as,

$$W_{2n,w} = i\frac{k}{\beta} \sum_i \exp\left(-i\frac{k}{\beta}(\xi_i - \xi_{TE})\right) \cdot W_{2n} \tag{44}$$

$$V_{2n,w} = i\frac{k}{\beta} \sum_i \exp\left(-i\frac{k}{\beta}(\xi_i - \xi_{TE})\right) \cdot V_{2n} \tag{45}$$

where ξ_i = $(X_o - X_i)$ is the relative upstream distance between the influencing and receiving elements

and ξ_{TE} = $(X_o - X_{TE})$ is the relative upstream distance between the receiving element and center of the trailing edge.

For n = 0, 1, 2, etc. the expressions for $W_{2n,w}$ and $V_{2n,w}$ are the same as for the lifting surface elements. The summation in Equations (44) and (45) denotes the contribution from all the wake elements between the trailing edge and the intersection of the Mach hyperbola with the wake sheet (see Figure 3).

Finally, the modified normal wash distribution using Equation (6) may be expressed in matrix form

$$\frac{d\tilde{\eta}}{dT} e^{ik'MX_o} = [W]\left\{\frac{\partial K}{\partial X}\right\} + [W_w]\left\{K_{TE}\right\} \tag{46}$$

The trailing edge values of the velocity potential K_{TE} can be approximated by

$$K_{TE} = [\bar{X}]\left\{\frac{\partial K}{\partial X}\right\} \tag{47}$$

where the transformation matrix $\bar{X}$ is given by

$$[\bar{X}] = \begin{bmatrix} t_1 & & \\ & t_2 & \\ & & \ddots\ t_r \end{bmatrix} \tag{48}$$

in which

$$t_r = [\Delta X_o, \Delta X_1 \ldots . \Delta X_p]_r \tag{49}$$

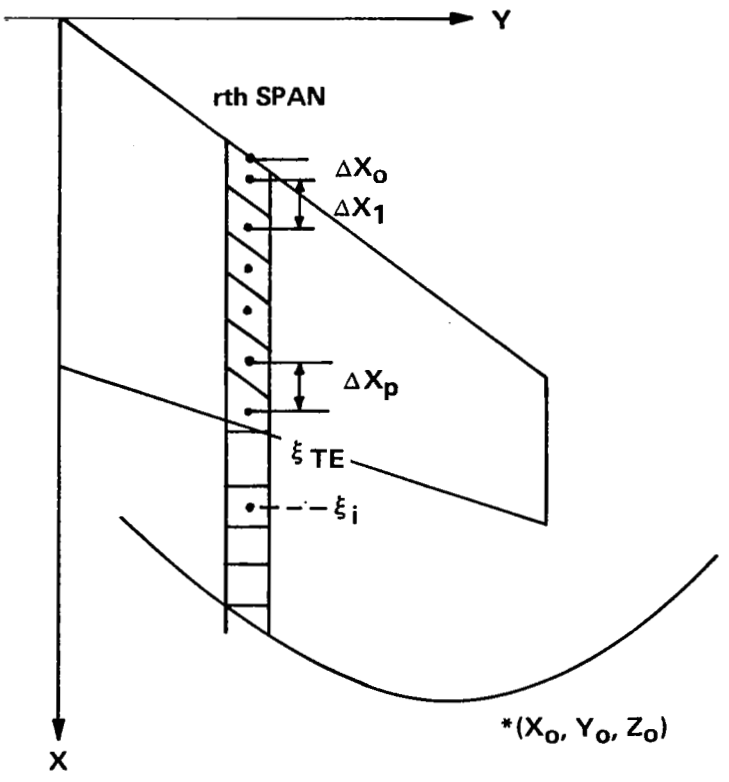

Figure 3. Consideration of Wake Sheet

t_r is a row vector defining the distances between the centers of the elements in the rth span from which trailing edge the wake sheet emanates (see Figure 3).

Using Equation (47), the modified velocity potential gradient can be related to the given boundary conditions as;

$$[W + W_w \cdot \bar{X}] \left\{ \frac{\partial K}{\partial X} \right\} = \frac{d\tilde{\eta}}{dT} e^{ik'MX_o} \tag{50}$$

Calculation of the Velocity Potential

Equation (50) can be solved for the velocity potential gradient $\frac{\partial K}{\partial X}$. It is then desired to determine K and subsequently the velocity potential difference $\Delta\phi = \phi_u - \phi_\ell$.

From Equation (2) et seq ,

$$\frac{\partial K}{\partial X} = \frac{1}{2\pi}\left(\frac{\partial \Delta\varphi}{\partial X} + ik'M\Delta\varphi\right) e^{ik'MX} \tag{51}$$

where $\Delta\varphi = \frac{\Delta\phi}{U\ell}$ is the nondimensional velocity potential difference.

Then

$$\frac{\partial \Delta\varphi}{\partial X} + ik'M\Delta\varphi = \psi \tag{52}$$

with

$$\psi = 2\pi \frac{\partial K}{\partial X} e^{-ik'MX} \tag{53}$$

Since $\Delta\varphi = 0$ at the leading edge, the solution to Equation (52) is given by

$$\Delta\varphi(X) = e^{-ik'MX} \sum_{\substack{\text{Chordwise} \\ \text{Elements}}} \int \psi(\xi) e^{ik'M\xi} d\xi \tag{54}$$

If ψ is expressed linearly between two element centers, Equation (54) can be integrated in a closed form between element centers, and the contributions summed. Finally, K is determined from Equation (2).

Calculation of the Generalized Forces

The lift on an element dx dy of the wing's surface is denoted by $\tilde{\ell}(x,y) \exp(ikT)$ and hence

$$\tilde{\ell}(x,y)\, dx\, dy = \ell^2 \beta \tilde{\ell}(X,Y)\, dX\, dY \tag{55}$$

where the lift distribution

$$\tilde{\ell}(X,Y) = 2\pi \frac{\rho U^2}{\beta} \left[\frac{\partial K}{\partial X} - \frac{ikK}{\beta} \right] e^{-ik'MX} \tag{56}$$

By the principle of virtual work, the generalized aerodynamic influence coefficient (AIC) can be written as

$$\tilde{Q}_{ij} = 4\pi \sum_{E} \tilde{\eta}_i \left(\frac{\partial K_j}{\partial X} - \frac{ikK_j}{\beta} \right) A_E e^{-ik'MX_j} \tag{57}$$

where $\tilde{Q}_{ij}$ is the nondimensional form of the coefficients defined by

$$Q_{ij} = q\ell^3 \tilde{Q}_{ij} \tag{58}$$

In the above equation, A_E is the area of a quadrilateral element of the wing and the contributions from all such elements of both sides of the wing are summed.

COMPUTATIONAL METHOD

This section briefly describes the idealization of the interacting wing surfaces, numerical calculation of the velocity components and the solution procedure. More detailed information is contained in the user's and programmer's manuals (refs. 26 and 27).

Idealization of Lifting Surfaces

The choice of the grid system plays an important role in the numerical computation of the unsteady aerodynamic coefficients in a supersonic flow field. Triangular, rectangular, quadrilateral and Mach characteristic grids have been employed in the supersonic analysis (e.g., references 11, 13, 14, 17, etc.). While well conditioned and more efficient calculations result from the grids based partly on Mach characteristic lines, as shown in Figure 4, the automated generation of such elements for a complex configuration such as multiple wings with control surfaces is difficult and proved beyond the scope of the current work.

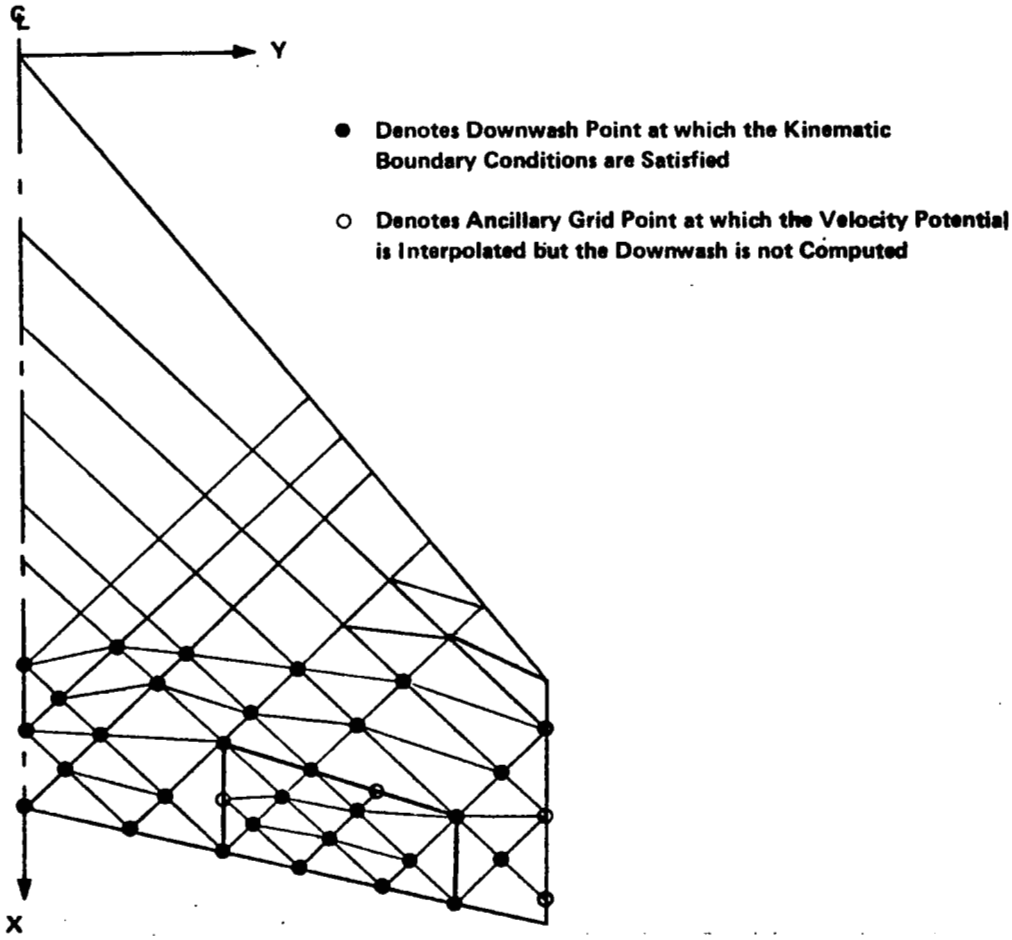

Figure 4. Typical Characteristic Grid Idealization With Control Surface

In the present development, trapezoidal elements have been chosen as the basis to model the interacting wing configurations with control surfaces. All the elements are assumed to have two sides parallel to the free stream. Figure 5 shows the idealization of a typical wing with control surfaces. As previously indicated, this element type has specific advantages for the performance of the recurring line integrals around the perimeter.

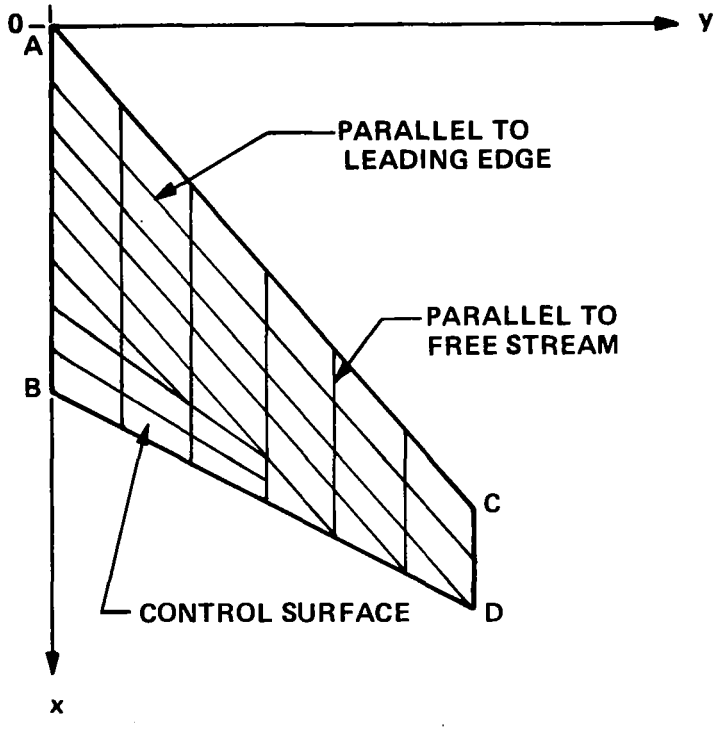

Figure 5. Idealization of Wing Planform for Constant Potential Gradient Method

Numerical Computation of the Integrals

Integrals of the velocity components given by Equations 9, 25, 27 and 32 through 40, are performed for all influencing elements in the dependence domain, with respect to a receiving point at the center of an element. These integrals are taken along the contour of each element. Since the sides of the elements are parallel to the streamlines, numerical line integrals are performed only along leading and trailing edges of the elements. Furthermore, all the integrals vanish on the Mach cone and the need for determining the hyperbolic curves of intersection of the cone with the lifting surface is avoided. In the case of partial elements, the line integration beyond the Mach hyperbola is zero.

The velocity influence coefficients $W_{ji,2n}$ which are independent of the reduced frequency k are first evaluated for each term in the series expansion. For n = 0 and n = 1, the integrals are easily

expressed in closed form, while for higher order terms, say $n \geq 2$, closed form expressions exist but are increasingly complex. Hence it is more economical to evaluate these integrals by numerical methods.

At low Mach numbers and for large reduced frequencies, convergence of this series is poor for far field elements. Numerical difficulties were also encountered in the evaluation of I_{2n} integrals given by Equation (28) since the magnitudes of the I_{2n} terms became very large. However, for a given frequency, the total value of the influence coefficient, i.e.,

$$W_{ji} = \sum_{n=0,1,2\ldots} C_{2n} W_{ji,2n} \tag{59}$$

approaches an asymptotic value for far field elements. Figure 6 shows a typical distribution of the velocity coefficients for various chordwise and spanwise positions (ξ, η) of an influencing element i with respect to a receiving element j.

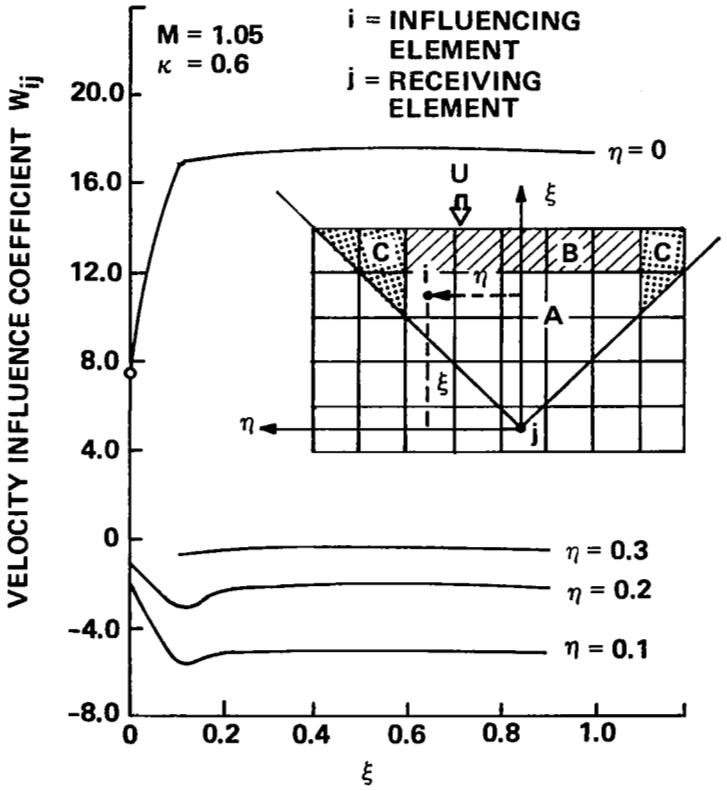

Figure 6. Asymptotic Nature of Far Field Elements

For $\eta = 0$, the asymptotic value is seen to have been obtained for all upstream elements beyond $\xi \geq 0.4$ (region B in Figure 6). A similar asymptotic trend is seen for elements at other span stations such as $\eta = 0.1, 0.2, 0.3$, etc., with a drastic reduction in magnitude of the velocity components. This behavior is discussed for rectangular elements in the Appendix.

A dependence domain C with respect to the receiving point j (Figure 6) can be constrained by specifying a certain order of magnitude of the velocity components W_{ij} in relation to W_{jj} such that the total solution does not vary by more than, say, 2 percent. Thus, the actual computation can be performed only for the region A while the upstream region B is represented by the asymptotic values obtained in the region A. In this way increased computational economy has been achieved in the development of the computer program (see references 26 and 27). This also eliminates the numerical difficulty encountered in the computation of I_{2n} integrals for the far field elements.

Solution Procedure

Accurate determination of unsteady aerodynamic forces on lifting surfaces with controls requires that the configuration be defined by a large number of elements which prevents the matrix relation given by Equation (50) from being solved economically by inversion techniques. Iterative methods have been developed to solve such large order linear systems on digital computers of limited memory size. In the present work, an iterative technique developed by Bratkovich and Marshall (reference 28) has been chosen as the most efficient one. This method is based on the successive-over-relaxation technique, without the need to determine the relaxation factor by trial and error runs.

After the frequency independent coefficients have been determined, the total solution is obtained for any frequency within a required range. Computational efficiency can be increased by using the previously determined solutions as the starting vectors for different frequencies.

Reference 27 discusses in greater detail the cpu time taken for operations such as:

(1) determination of the coefficients
(2) decomposition of the matrix
(3) solution for each mode, and
(4) solution for each frequency, etc.

RESULTS AND DISCUSSIONS

To assess the solution accuracy and the versatility of the potential gradient method, a number of calculations have been performed on an IBM 360/65 computer and compared with available results. In all the cases considered here, the wing planforms were represented by trapezoidal finite elements. Generalized aerodynamic coefficients and pressure distributions were calculated for various reduced frequencies and Mach numbers. The examples include planar and nonplanar configurations with control surfaces.

Isolated Wings

Double Delta Wing

The wing planform (Figure 7a) was represented by 150 elements, with 15 span stations. The pressure distributions along the span for various chord stations are compared with the results of

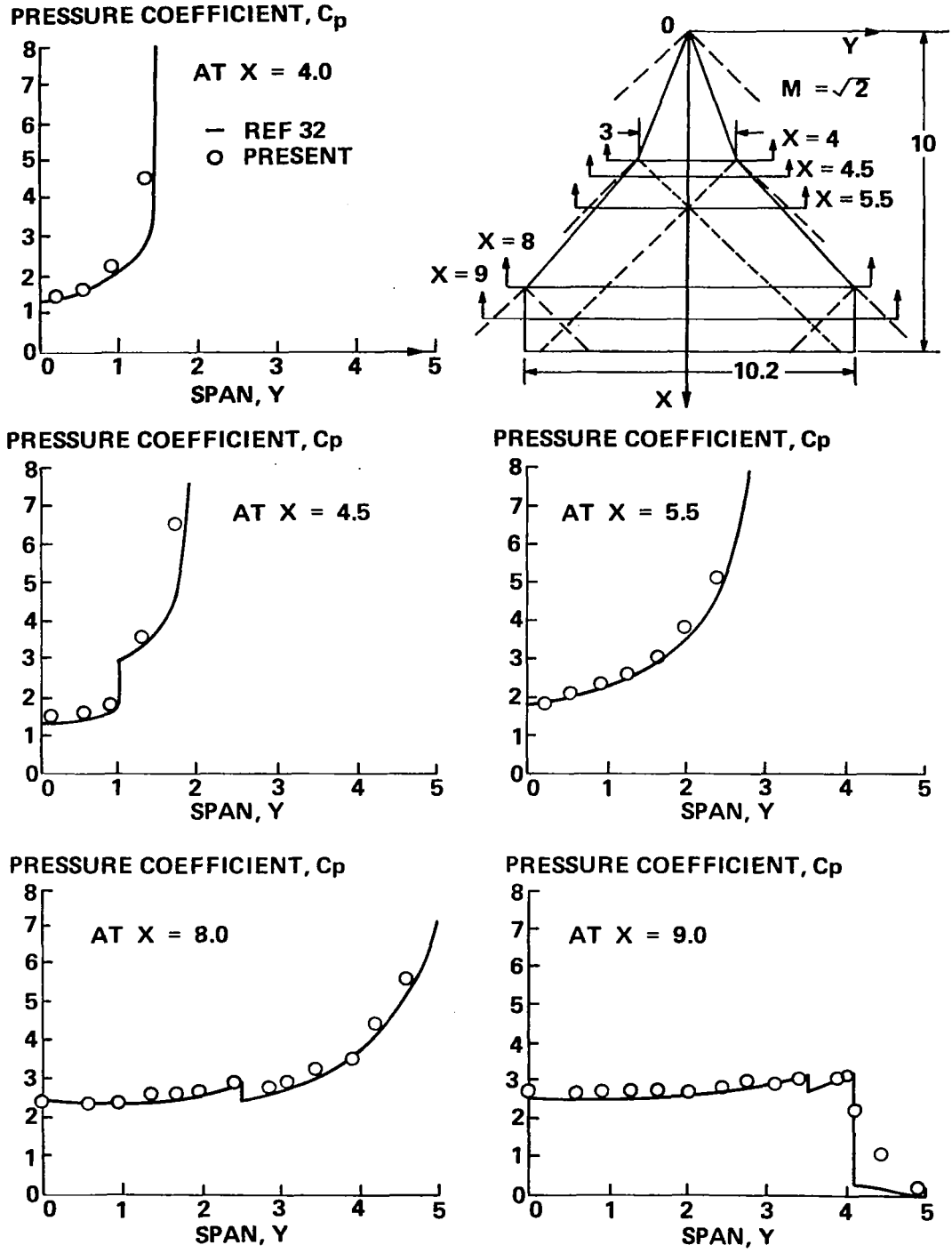

Figure 7. Double Delta Wing at M = $\sqrt{2}$. Steady State Pressures

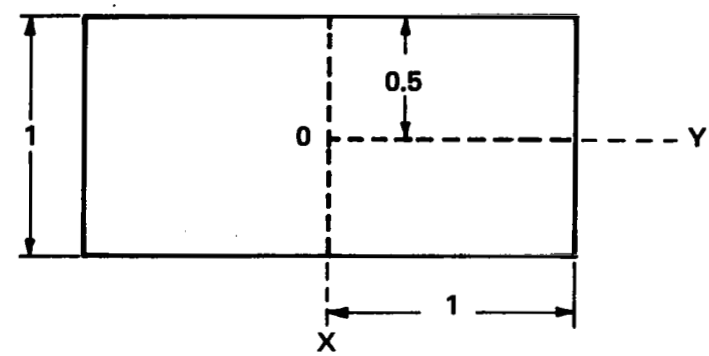

(a) AR = 2 RECTANGULAR WING

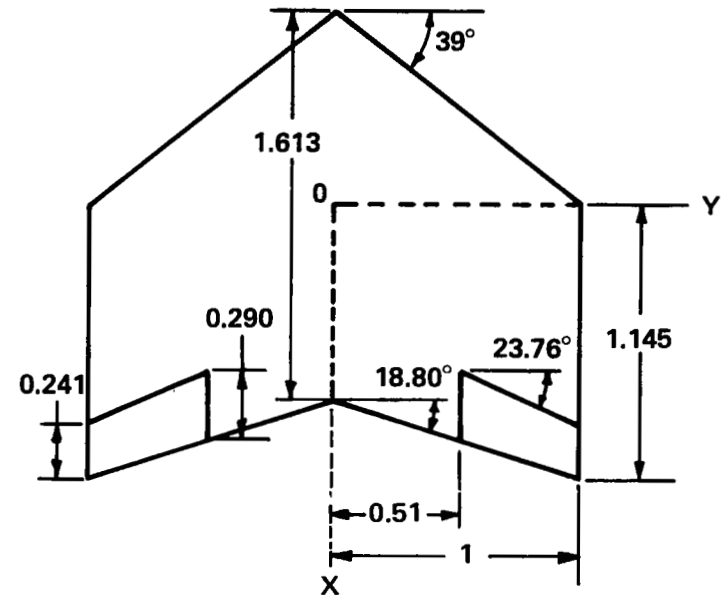

(b) AR = 1.45 TAPERED SWEPT-BACK WING

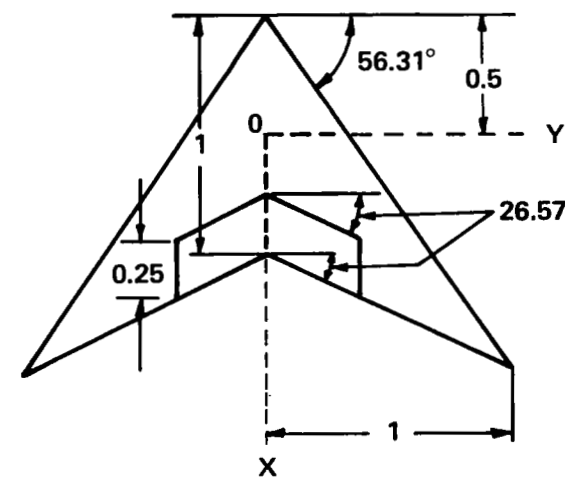

(c) AR = 4 ARROWHEAD WING

Figure 8. AGARD Planforms

ref. 29. The correlation is very good, except at the tip section (see Figure at X = 9.0), where the large pressure discontinuity is smeared by the discrete element approach.

Rectangular and Arrowhead Wings

The generalized aerodynamic coefficients for rectangular and arrowhead wings (Figure 8a and 8c) for heave and pitch motions are, in Tables 1 and 2, compared with Fenain's (ref. 22) and Stark's (ref. 13) methods as reported by Woodcock in ref.21. The number of elements used in chord and span directions are shown in the tables. The generalized aerodynamic coefficients determined for the Mach number range M = 1.04 to M = 2.0 and reduced frequencies k = 0, 0.5, and 1.0, are seen to be in very good agreement, in spite of fewer elements used in the present method.

AGARD Swept Wing With Control Surface

Figure 8b shows the planform of the AGARD swept wing with control surface. The wing was represented by 147 trapezoidal elements with 15 of them on the Control Surface. The oscillating modes of the wing considered in the present calculations were:

1. Heave $\eta_1 = 1.0$
2. Pitching about the mid-chord (C/2) $\eta_2 = X - C/2$
3. Chordwise bending $\eta_3 = (X - C/2)^2$
4. Flapping of control surface.

The generalized aerodynamic coefficients were calculated at M = 1.2, and reduced frequencies k = 0.5 and 1.0.

Table 3 shows the comparison of the present results with those of refs. 13 and 22. In spite of the large difference in the number of elements used in the present and the referenced methods, the generalized aerodynamic coefficients are in good agreement, except for the loss of accuracy in the small order terms.

When the magnitudes of the real and imaginary parts of a complex number differ significantly, it is better to compare two complex numbers using their magnitudes and phases. For example, amplitudes of Q_{13} and Q_{14} are in good agreement while their phase angles differ only by a fraction of a degree.

Interacting Wings

Rectangular Wing Folding at 50% Semi Span

In order to check the accuracy of the out of plane velocity components derived in the present approach, a rectangular wing of aspect ratio 4 folded at 50 percent of semi span was considered. Lift curve slopes at $M = \sqrt{2}$ for various fold angles were calculated, and indicate excellent agreement with the theoretical values ref. 30 (Figure 9). Mach box results of ref. 30 shown in this figure, overestimate the values of lift curve slopes at low fold angles and underestimate them at high fold angles.

TABLE 1

AGARD RECTANGULAR WING (PLANFORM FIG. 8 (a))
MODES $Z_1 = 1.0$ $Z_2 = X\text{-}C/2$ AR = 2.0

Mach No.	Methods (Matrix) or (Sp/Ch Pts.)*	Qij	k = 0		k = 0.3		k = 0.6	
			Re(Q)	Im(Q)	Re(Q)	Im(Q)	Re(Q)	Im(Q)
1.2	Present (49)	1,1			0.215	1.070	0.472	1.715
	M9 (34/26)**				0.205	1.060	0.749	1.820
	M19 (22/17)***				0.189	1.009	0.348	1.639
	Present	1,2	3.978		3.567	-0.593	2.938	-0.556
	M9		3.951		3.531	-0.545	3.058	-0.946
	M19		3.750		3.370	-0.500	2.840	-0.294
	Present	2,1			-0.001	-0.132	-0.096	-0.300
	M9				-0.005	-0.141	-0.026	-0.310
	M19				-0.005	-0.131	-0.107	-0.285
	Present	2,2	-0.370		-0.419	0.157	-0.403	0.440
	M9		-0.398		-0.446	-0.177	-0.427	0.350
	M19		-0.368		-0.411	-0.165	-0.380	0.450
1.05	Present (99)	1,1			0.008	1.128	0.158	2.065
	M9 (34/54)**				0.034	1.144	0.146	2.083
	M19 (14/22)***				0.019	1.088	0.124	1.997
	Present	1, 2	3.880		3.955	0.255	3.781	-0.035
	M9		3.787		4.0	0.088	3.806	0.004
	M19		3.542		3.80	0.134	3.648	0.036
	Present	2,1			-0.200	-0.193	-0.3419	-0.200
	M9				-0.185	-0.204	-0.333	-0.251
	M19				-0.174	-0.197	-0.320	-0.244
	Present	2,2	-1.339		-0.544	0.837	-0.1616	0.797
	M9		-1.363		-0.590	0.790	-0.250	0.825
	M19		-1.293		-0.571	0.749	-0.247	0.790

* Spanwise and chordwise grid points

** As reported in Ref. 21 using the method of Ref. 22

*** As reported in Ref. 21 using the method of Ref. 13

TABLE 2. AGARD ARROW HEAD WING (FIG. 8 (c))

MODES: $Z_1 = 1.0$, $Z_2 = X\text{-}C/2$, AR = 4.0

Mach No.	Methods (Matrix Size or Sp/Ch Grid)*	Q_{ij}	k = 0		k = 0.5		k = 1.0	
			Re(Q)	Im(Q)	Re(Q)	Im(Q)	Re(Q)	Im(Q)
	Present (43)				0.046	0.6514	0.161	1.239
	M9 (34, 15)**				0.059	0.6085	0.198	1.136
	M19(40, 17)***	1, 1			0.055	0.6122	0.186	1.144
2.0	Present (43)	1, 2	1.334		1.306	0.1318	1.254	0.292
	M9 (34, 15)**		1.248		1.222	0.0766	1.164	0.190
	M19 (40, 17)***		1.255		1.228	0.0851	1.165	0.208
	Present (43)				0.027	0.236	0.094	0.436
	M9 (34, 15)				0.031	0.226	0.105	0.406
	M19 (40, 17)	2, 1			0.029	0.224	0.096	0.404
	Present (43)		0.489		0.474	0.0858	0.448	0.188
	M9 (34, 15)		0.471		0.457	0.0595	0.426	0.140
	M19 (40, 17)	2, 2	0.467		0.452	0.0650	0.419	0.151
	Present (110)				0.146	1.104		
	M9 (34, 35)				0.146	0.913		
	M19 (26, 26)	1. 1			0.136	0.887		
1.25	Present (110)		2.182		2.316	0.156		
	M9 (34, 35)		2.002		1.911	0.138		
	M19 (26, 26)	1, 2	1.936		1.852	0.147		
	Present (110)				0.089	0.442		
	M9 (34, 35)				0.075	0.330		
	M19 (26, 26)	2, 1			0.072	0.329		
	Present (110)	2, 2	0.858		0.949	0.101		
	M9 (34, 35)		0.758		0.710	0.100		
	M19 (26, 26)		0.748		0.705	0.102		

* Spanwise and chordwise grid points

** As reported in Ref. 21 using the method of Ref. 22

*** As reported in Ref. 21 using the method of Ref. 13

TABLE 3
AGARD SWEPT BACK WING WITH CONTROL (FIG. 8 (b))
MACH NO. = 1.2 TOTAL CPU = 306 SEC (IBM 360/65)

		k = 0.5			k = 1.0		
	i, j	Ref 22	Ref 13	Present	Ref 22	Ref 13	Present
	No. Elements	34 x 51	20 x 30	147	34 x 51	20 x 30	147
REAL (Q_{ij})	1, 1	0.0110	-0.0228	0.1758	-0.3690	-0.4042	-0.6150
	2, 1	-0.2780	-0.2832	-0.2332	-0.7220	-0.7085	-0.8567
	3, 1	-0.1620	-0.1643	-0.1193	-0.3500	-0.3397	-0.3840
	4, 1	-0.0100	-0.0090	-0.0094	-0.0230	-0.0222	-0.0186
	1, 2	3.8110	3.6714	3.515	4.1910	4.0734	4.0721
	2, 2	0.2870	0.2442	0.0906	0.8580	0.8016	0.8924
	3, 2	0.7160	0.6824	0.6056	0.9520	0.9106	0.9666
	4, 2	0.0200	0.0186	0.0131	0.0260	0.0235	0.0305
	1, 3	3.5220	3.3533	3.916	2.7140	2.5672	2.6444
	2, 3	2.8130	2.7026	2.958	2.2980	2.2108	2.0063
	3, 3	1.444	1.3568	1.547	1.2660	1.1923	1.1051
	4, 3	0.0850	0.0803	0.0672	0.0830	0.0784	0.0526
	1, 4	0.5900	0.5723	0.5563	0.5600	0.5437	0.5313
	2, 4	0.5320	0.5101	0.4984	0.5020	0.4834	0.4748
	3, 4	0.4830	0.4583	0.4494	0.4550	0.4332	0.4244
	4, 4	0.0530	0.0514	0.0448	0.0490	0.0478	0.0419
IMG (Q_{ij})/k	1, 1	3.4790	3.3506	3.2200	3.6460	3.5473	3.4314
	2, 1	0.0410	0.0084	0.1699	0.5440	0.5016	0.5390
	3, 1	0.5810	0.5532	0.4637	0.8420	0.8084	0.8644
	4, 1	0.0160	0.0146	0.0074	0.0250	0.0227	0.0311
	1, 2	1.6770	1.7325	1.2420	1.6100	1.5832	1.8967
	2, 2	2.4910	2.4589	2.4289	1.7880	1.7385	1.8345
	3, 2	1.3350	1.3055	1.2182	0.9040	0.8632	0.8562
	4, 2	0.0780	0.0738	0.0764	0.0610	0.0590	0.0485
	1, 3	-1.2090	-1.1954	-1.0223	0.1750	0.1563	-0.0139
	2, 3	-1.0740	-1.0507	-1.2672	0.1180	0.0996	0.0826
	3, 3	-0.2560	-0.2489	-0.3390	0.4570	0.4360	0.5124
	4, 3	0.0220	0.0198	-0.0049	0.0440	0.0412	0.0373
	1, 4	-0.0410	-0.0298	-0.0170	-0.0270	-0.0168	-0.0054
	2, 4	-0.0320	-0.0220	-0.0104	-0.0180	-0.0093	0.0010
	3, 4	-0.0260	-0.0149	-0.0173	-0.0120	-0.0023	-0.0059
	4, 4	0.0020	0.0032	0.0042	-0.0040	0.0052	0.0058

Note: Modes are defined in the text.

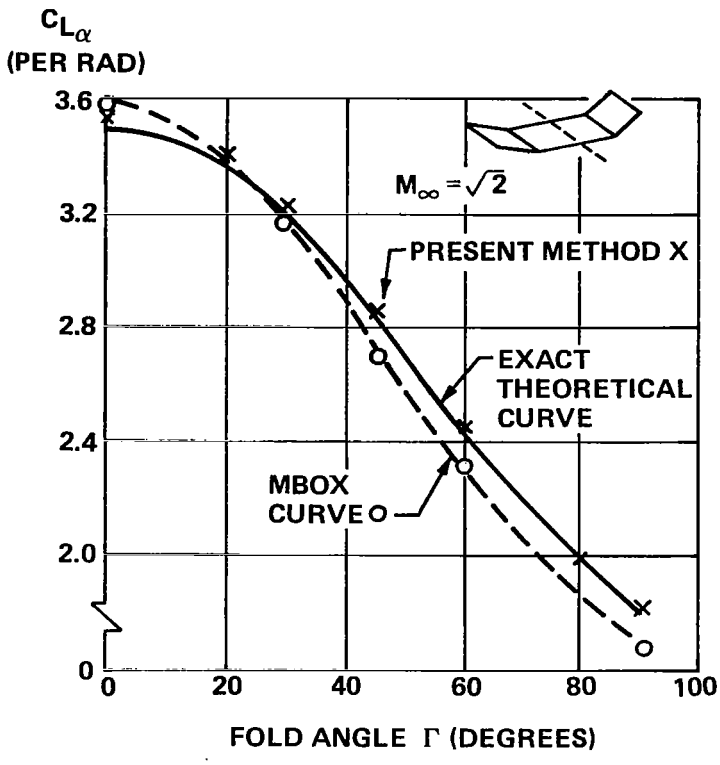

Figure 9. Lift Curve Slope For An Aspect Ratio 4.0 Rectangular Wing With Folded Tips

AGARD Wing-Tail Configuration

In the interacting case, the generalized aerodynamic coefficients were calculated for the AGARD wing-tail coplanar configuration (Z = 0) shown in Figure 10. Four antisymmetric modes of the form:

	Wing	Tail	Mode
η_1	Y(X-2.25|Y|-0.85)	0	wing twist
η_2	Y|Y|	0	wing bending
η_3		Y	tail roll
η_4		|Y| (X-3.35)	tail pitch

were considered.

The wing and tail were represented by 111 and 71 trapezoidal elements respectively. Generalized aerodynamic coefficients were calculated at M = 3.0 for reduced frequencies k = 0 and 1.5. Table 4 compares these results with those of ref. 24 and 31. The generalized aerodynamic loads on the wing due to wing modes, and on the tail due to tail modes are in excellent agreement with the referenced methods. However, the interference effects, i.e., loads on tail due to wing modes,

	x	y	z
a	0	0	0
b	2.25	0	0
c	2.75	1.00	0
d	3.70	1.00	0
e	2.70	0	0
f	4.00	0	0
g	3.90	1.00	0
h	4.25	1.00	0
e'	3.10	0	0.60
f'	4.40	0	0.60
g'	4.30	1.00	0.60
h'	4.65	1.00	0.60
e''	3.55	0	1.20
f''	4.85	0	1.20
g''	4.75	1.00	1.20
h''	5.10	1.00	1.20
e'''	2.70	0	0
f'''	4.00	0	0
g'''	3.90	1.00	0.50
h'''	4.25	1.00	0.50
i	2.50	0	0
j	4.20	0	0
k	3.70	0	1.20
ℓ	4.60	0	1.20

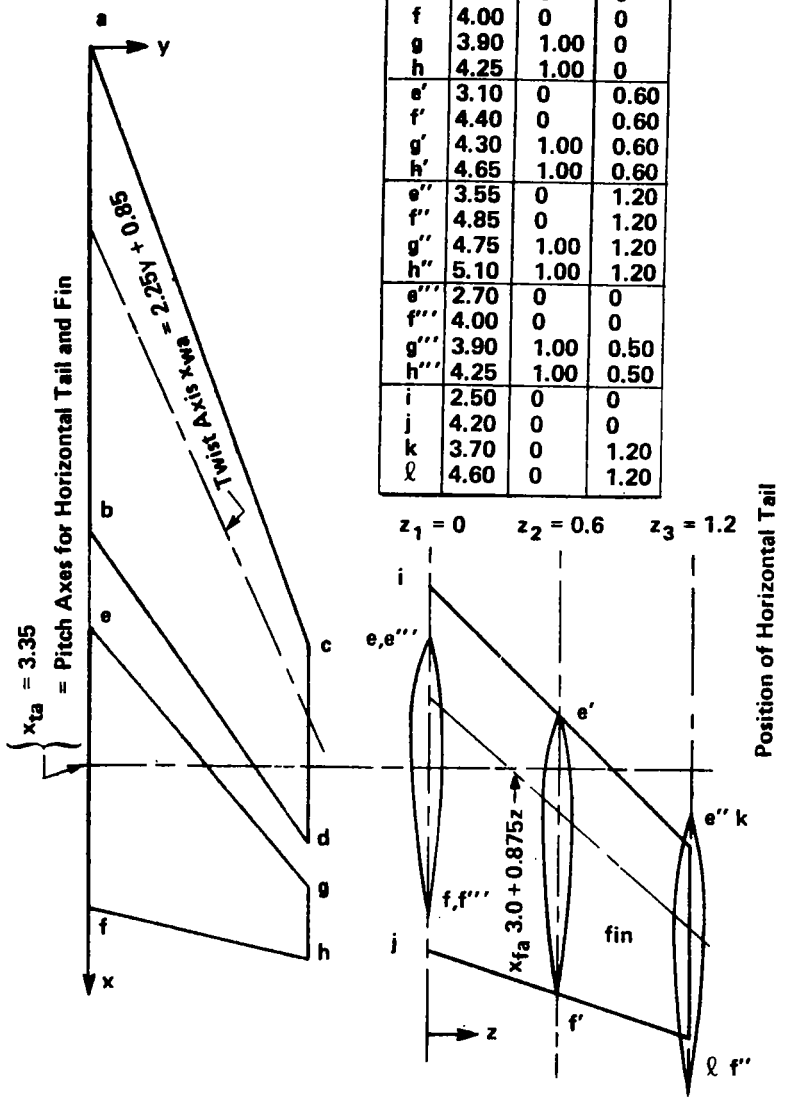

Figure 10. AGARD Wing-Horizontal Tail-Vertical Fin Combination

TABLE 4
AGARD WING-TAIL INTERFERENCE M = 3.0 Z = 0.0
NO. ELEMENTS = 111 (WING) + 71 (TAIL) TOTAL CPU = 246 SEC (IBM 360/65)

		k = 0.0			k = 1.5		
	i, j	Ref 24	Ref 31	Present	Ref 24	Ref 31	Present
REAL (Q_{ij})	1, 1	-0.0226	0.0189	-0.0187	0.0966	0.1066	0.0901
	2, 1	0.3035	0.2789	0.3287	0.3846	0.3238	0.3895
	3, 1	-0.2152	0.2226	-0.1075	-0.0394	0.1438	-0.0695
	4, 1	-0.1550	-0.0006	-0.0843	-0.0147	0.1438	-0.0360
	1, 2				-0.0700	-0.0668	-0.0819
	2, 2				-0.0759	-0.0530	-0.0888
	3, 2				-0.1531	0.1701	-0.0400
	4, 2				-0.1033	0.0216	-0.0179
	1, 3						
	2, 3						
	3, 3				0.0168	0.0127	0.0140
	4, 3				0.0050	0.0008	0.0032
	1, 4						
	2, 4						
	3, 4	0.4650	0.4338	0.4756	0.4517	0.3859	0.4541
	4, 4	0.2882	0.3018	0.2904	0.2965	0.2578	0.2903
IMG (Q_{ij})/k	1, 1				0.1486	0.1345	0.1593
	2, 1				0.0890	0.0865	0.1083
	3, 1				0.0769	-0.0612	0.0007
	4, 1				0.0559	-0.0612	0.0008
	1, 2				0.0309	0.0463	0.0300
	2, 2				0.2363	0.2040	0.2498
	3, 2				0.0239	0.0670	-0.0003
	4, 2				0.0197	0.0398	0.0030
	1, 3						
	2, 3						
	3, 3				0.2560	0.2283	0.2635
	4, 3				0.1786	0.1669	0.1820
	1, 4						
	2, 4						
	3, 4				0.1632	0.1518	0.1820
	4, 4				0.2188	0.1910	0.2300

Note: Modes are defined in the text.

do not agree in magnitude among the methods compared. The discrepancy may be resolved by conducting additional correlation with other methods.

Tail-Fin Configuration

A T-tail configuration, with tail mounted on fin a $Z_3 = 1.2$ as shown in Figure 10 was considered as the next example with the following modes of oscillation:

	Tail	Fin	Mode
η_1 =	0,	Z^2	Fin bending
η_2 =	0,	Z(X-0.875Z-3.0)	Fin twist
η_3 =	Y,	0	Tail roll

Tail and fin were represented by 42 and 63 trapezoidal elements. Generalized aerodynamic coefficients were calculated at M = 1.6 for reduced frequencies k = 0 and 1.5, and are given in Table 5. It was intended to compare with the results of reference 32. For some reason Table Q3.11 of reference 32 was not available in that report. However, the corresponding result with fin reflection is shown in Table 5. There seems to be no agreement in any of the generalized aerodynamic coefficients. The results of ref.32 appear to be 2 to 3 times higher than the values obtained from the present method with no fin reflection.

TABLE 5
AGARD TAIL - FIN INTERFERENCE M = 1.6 Z = 1.2
NO. ELEMENTS = 42 (TAIL) + 63 (FIN) TOTAL CPU = 93 SEC (IBM 360/65)

		k = 0.0		k = 1.5	
	i, j	Ref. 31*	Present	Ref. 31*	Present
Real (Q_{ij})	1, 1			1.3389	-0.0125
	2, 1			0.0664	-0.0605
	3, 1			0.4630	0.056
	1, 2	2.7068	0.8089	1.4164	0.6516
	2, 2	0.3511	0.0970	0.2823	0.1031
	3, 2	0.5621	0.2258	0.1392	-0.1359
	1, 3			0.1251	0.0370
	2, 3			0.0211	0.1795
	3, 3			0.0350	0.0025
IMG (Q_{ij})/k	1, 1			4,7124	0.5200
	2, 1			0.1324	0.0449
	3, 1			1.6933	0.1209
	1, 2			-0.4249	0.1430
	2, 2			0.1817	0.1643
	3, 2			-0.2333	0.0047
	1, 3			1,6239	0.0527
	2, 3			0.0074	0.0166
	3, 3			0.6700	0.4457

*The results of Reference 31 were obtained with fin reflection.

Wing-Tail-Fin Configuration

This was the last in the series of the examples considered. The tail was placed at Z = 0. Four modes;

i) wing twist
ii) tail pitch
iii) fin bending, and
iv) fin twist,

as defined in the previous examples were considered. Generalized aerodynamic coefficients were calculated at M = 3.0 for frequencies k = 0 and 1.5 and are presented in Table 6. For this configuration, no other results are available for comparison.

TABLE 6
AGARD WING - TAIL - FIN INTERFERENCE M = 3.0 Z = 0
NO. ELEMENTS = 73 (WING) + 70 (TAIL)+110 (FIN) TOTAL CPU = 203 SEC (IBM 360/65)

	k = 0.0		k = 1.5	
i, j	Real (Q_{ij})	IMG (Q_{ij})/k	Real (Q_{ij})	IMG (Q_{ij})/k
1, 1	-0.0202		0.0839	0.1641
2, 1	-0.1333		-0.1779	0.1444
3, 1	-0.0980		0.0492	0.0066
4, 1	-0.0460		0.0240	0.0185
1, 2				
2, 2	0.3420		0.3137	0.2160
3, 2	-0.01756		0.0042	0.0084
4, 2	-0.0414		-0.0059	0.0170
1, 3				
2, 3			-0.0046	-0.0006
3, 3			-0.0420	0.2918
4, 3			-0.0217	0.0361
1, 4				
2, 4	-0.0144		-0.0017	0.0059
3, 4	0.3400		0.03314	0.0780
4, 4	0.0545		0.0551	0.0711

Influence of Element Mismatch on Pressure Distribution

The lifting surfaces are commonly represented by discrete elements bounded by continuous lines drawn from root chord to tip chord and leading edge to trailing edge. For highly tapered wings, this may result in an undesirable concentration of small elements at the tip. Elements of nearly equal areas could be obtained by terminating some lines at partial span stations (e.g., see the control surface in Figure 5).

In subsonic doublet methods such a discontinuity creates undesirable fluctuations in the pressure distribution (ref. 2). Some misgivings were voiced concerning similar effects in the present method. They do not seem to be significant as evidenced by the following examples.

Figure 11a and b shows the chordwise pressure distribution at two spanwise stations adjacent to the leading edge crank of the double delta wing of Figure 7. Two cases of 'element mismatch' are shown. In both the cases the pressure distributions are relatively smooth. Figure 11b also shows the pressure distribution with element downwash points located at 0.75 and 0.8 of the element chords. No significant effect was observed. However, in the case of wings such as Figure 8c, pressure distributions with the downwash point taken at 0.5 of the element chord gave unsatisfactory results. In general, a choice of downwash point anywhere between 0.6 to 0.8 of the element center chord should give satisfactory results.

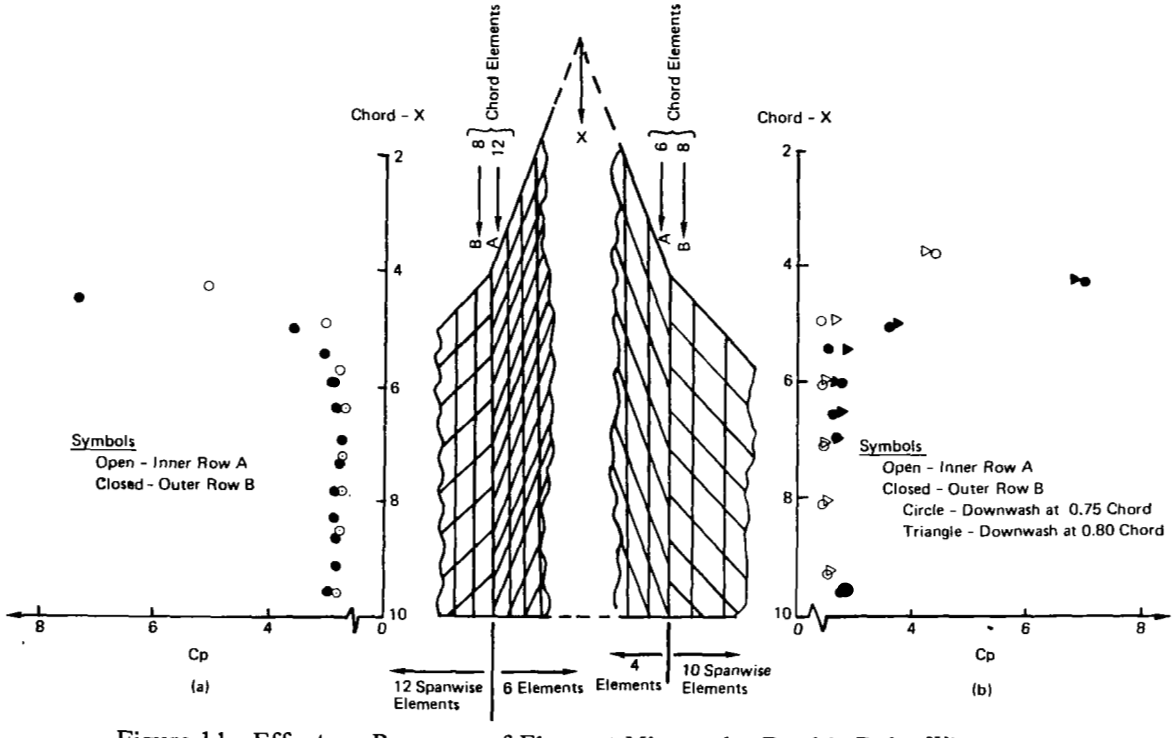

Figure 11. Effect on Pressures of Element Mismatch - Double Delta Wing

CONCLUSIONS

The potential gradient approach, unlike the pressure potentials, results in simplified integral formulae. By expanding the kernel, the singular integrals have been evaluated in closed form without the need for principal or finite part integral techniques. Integrals vanish on the Mach cone and the need for determining the hyperbolic curves of intersection of the cone with the lifting surface is avoided. Furthermore, idealization of lifting surfaces by trapezoidal finite elements with two sides parallel to the streamlines, requires numerical integrals to be performed along the other two sides

only. Such elements are amenable to automatic grid generation schemes. Comparable results to other methods are obtained with far fewer elements.

REFERENCES

1. Jones, W.P., "Supersonic Theory for Oscillating Wings of any Planform," Brit. A.R.C R&M 2655, June 1948.
2. Giesing, J.P., Kalman, T.P. and Rodden, W.P., "Subsonic Unsteady Aerodynamics for General Configurations," AFFDL-TR-71-5, Part I, November 1971, AFFDL-TR-71-5, Part II, April 1972.
3. Garrick, I.E., and Rubinow, S.I., "Theoretical Study of Air Forces on an Oscillating or Steady Thin Wing in a Supersonic Main Stream," NACA Report 827, 1947.
4. Ashley, H., "Supersonic Airloads on Interfering Lifting Surfaces by Aerodynamic Influence Coefficient Theory," Boeing Report D2-22067, Nov. 1962.
5. Watkins, C.E. and Berman, J.H., "On the Kernel Function of the Integral Equation Relating Lift and Downwash Distributions of Oscillating Wings in Supersonic Flow," NACA Rep. 1257, 1956.
6. Harder, R.L. and Rodden, W.P., "Kernel Function for Non-Planar Oscillating Surfaces in Supersonic Flow," Jour. of Aircraft, Vol. 8, No. 8, Aug. 1971, pp. 667-679.
7. Heaslet, M.A., Lomax, H. and Jones, A.L., "Volterra's Solution of the Wave Equation as Applied to Three-Dimensional Supersonic Airfoil Problems," NACA Report 889, 1947.
8. Richardson, J.R., "A Method for Calculating the Lifting Forces on Wings (Unsteady Subsonic and Supersonic Lifting-Surface Theory)," Brit. A.R.C., R&M No. 3157, 1955.
9. Cunningham, H.J., "Improved Numerical Procedure for Harmonically Deforming Lifting Surfaces from the Supersonic Kernel Function Method," AIAA Jour., Vol. 4, No. 11, Nov. 1966 pp. 1961-1968.
10. Cunningham, A.M., Jr., "A Kernel Function Method for Computing Steady and Oscillatory Supersonic Aerodynamics with Interference," AIAA Paper No. 73-670, AIAA 6th Fluid and Plasma Dynamics Conference, Palm Springs, Californina, July 16-18, 1973.
11. Ii, J.M., Boreland, C.J. and Hogley, J.R., "Prediction of Unsteady Aerodynamic Loadings of Non-Planar Wings and Wing-Tail Configurations in Supersonic Flow. Part I - Theoretical Development, Program Usage, and Application," USAF AFFDL-TR-71-108, Part I, March 1972.
12. Kramer, G.D. and Kaylon, G.E., "Prediction of Unsteady Aerodynamic Loadings of Non-Planar Wings and Wing-Tail Configurations in Supersonic Flow. Part II," USAF AFFDL-TR-71-108, Part II, March 1972.
13. Stark, V.J.E., "Calculation of Aerodynamic Forces on Two Oscillating Finite Wings at Low Supersonic Mach Numbers," SAAB Tech. Note TN 53, 1964.
14. Appa, K., "Kinematically Consistent Unsteady Aerodynamic Coefficients in Supersonic Flow," Intl. Jnl. for Numerical Methods in Engineering, Vol. 2, pp. 495-507, October 1970. (Also National Aeronautical Laboratories NAL TN-9, India, March 1968.)

15. Appa, K. and Smith, G.C.C., "Further Developments in Consistent Unsteady Supersonic Aerodynamic Coefficients," AIAA, Journal of Aircraft, Vol. 9, No. 2, February 1972.
16. Appa, K. and Smith, G.C.C., "Development and Applications of Supersonic Unsteady Consistent Aerodynamics for Interfering Parallel Wings," NASA CR-2168, March 1973.
17. Allen, D.J., and Sadler, D.S., "Oscillatory Aerodynamic Forces in Linearized Supersonic Flow for Arbitrary Frequencies, Planforms and Mach Numbers," Brit. A.R.C. R&M No. 3415, 1963.
18. Woodcock, D.L. and York, E.J., "A Supersonic Box Collocation Method for the Calculation of Unsteady Airforces of Tandem Surfaces." Proceedings of AGARD Symposium on Unsteady Aerodynamics for Aeroelastic Analyses of Interfering Surfaces. AGARD-CP-80-71, 1971.
19. Chen, L.T., Suciu, E.O. and Morino, L., "A Finite Element Method for Potential Aerodynamics around Complex Configurations," AIAA Paper No. 74-107, AIAA 12th Aerospace Sciences Meeting, Washington, D.C., Jan. 30-Feb. 1, 1974.
20. Appa, K. and Smith, G.C.C., "Finite Element Approach to the Integrated Potential Formulation of General Unsteady Supersonic Aerodynamics," NASA-CR-112296, 1973.
21. Woodcock, D.L. (Ed.), "A Comparison of Methods used in Lifting Surface Theory," Supplement to the Manual on Aeroelasticity, Pt. VI, NATO-AGARD Report No. 583, 1971.
22. Fenain, M. and Guiraud-Vallee, D., "Numerical Calculations of Wings in Steady or Unsteady Supersonic Flow, Part 1; Steady Flow: Part 2; Unsteady Flow," Recherche Aerospatiale No. 115, 1966-67.
23. Appa, K. and Jones, W.P., "Integrated Potential Formulation of Unsteady Supersonic Aerodynamics for Interacting Wings," Journal of Aircraft, AIAA, Vol 13, No. 9, September 1976.
24. Pollock, S.J. and Huttsell, L.J., "Applications of Three Unsteady Aerodynamic Load Prediction Methods," AFFDL TR-73-147, May 1974.
25. Jones, W.P. and Appa, K., "Unsteady Supersonic Aerodynamic Theory by the Method of Potential Gradient." AIAA Journal, Vol 15, No. 1, January 1977.
26. Crill, W. and Dale, B., "A General Purpose Computer Program for Interacting Supersonic Configurations - User's Manual," NASA-CR-145128 April 1977.
27. Crill, W. and Dale, B., "A General Purpose Computer Program for Interacting Supersonic Configurations - Programmer's Manual," NASA-CR-145127 April 1977.
28. Bartkovich, K. and Marshall, F.J., "Iterative Techniques for the Solutions of Large Linear Systems in Computational Aerodynamics," Journal of Aircraft, Vol. 12, No. 3, Feb. 1975, pp. 116-118.
29. Cohen, D. and Friedman, M.D., "Theoretical Investigation of the Supersonic Lift and Drag of Thin, Sweptback Wings with Increased Sweep near the Root," NACA TN 2959, June 1953.
30. Donato, V.W. and Huhn, C.R., Jr., "Supersonic Unsteady Aerodynamics for Wings with Trailing Edge Control Surfaces and Folded Tips," AFFDL-TR-68-30, August 1968.
31. Tsen, K. and Morino, L., "A New Unified Approach for Analyzing Wing-Body-Tail Configurations with Control Surfaces," AIAA Paper No. 76-418, AIAA 9th Fluid and Plasma Dynamics Conference, San Diego, CA., July 14-16, 1976.
32. Rodden, W.P., "A Comparison of Methods Used in Interfering Lifting Surface Theory," Supplement to the Manual on Aeroelasticity, Volume VI, AGARD-R-643, 1976.

APPENDIX
BEHAVIOR OF THE FAR FIELD ELEMENTS

In Figure 6, it appears that the velocity influence coefficient has an asymptotic trend for increasing ξ.

Suppose in Figure 6, a rectangular sending element has sides $(2\epsilon, 2\gamma)$ and coordinates (ξ, η) such that $\frac{\epsilon}{\xi}, \frac{\gamma}{\eta}$ are small. For this box, approximately

$$W_{box} = \sum_n C_{2n} \left[\left[I_{2n}(\xi, \eta) \right]_{\xi - \epsilon}^{\xi + \epsilon} \right]_{\eta - \gamma}^{\eta + \gamma} \tag{A-1}$$

$$\simeq 2\epsilon \sum_n C_{2n} \left[\frac{\partial I_{2n}}{\partial \xi} \right]_{\eta - \gamma}^{\eta + \gamma} \tag{A-2}$$

Now this may be shown proportional to

$$2\epsilon \left[-\frac{\sqrt{1 - \left(\frac{\eta}{\xi}\right)^2}}{\eta} - \frac{k'^2}{2} \left\{ \eta L + \xi \sin^{-1}\left(\frac{\eta}{\xi}\right) \right\} + \frac{k'^4}{16} \xi^2 \eta + \cdots \right]_{\eta - \gamma}^{\eta + \gamma} \tag{A-3}$$

For $\eta = 0$ (ξ not small),

$$W_{box} \simeq 4\epsilon\gamma \left[-\frac{\sqrt{1 + \left(\frac{\gamma}{\xi}\right)^2}}{\gamma} - \frac{k'^2}{2} \left\{ \gamma \ell n \frac{2\xi}{\gamma} + \xi \sin^{-1} \frac{\gamma}{\xi} \right\} + k'^4 \frac{\xi^2 \gamma}{16} + \cdots \right] \tag{A-4}$$

For $\eta \neq 0, \left(\frac{\gamma}{\eta} \sim \frac{1}{2}, \frac{1}{4}, \frac{1}{6} \text{ etc.} \right)$

$$W_{box} \simeq 4\epsilon\gamma \left[\frac{1}{\eta^2} \left\{ \frac{1}{\sqrt{1 - \left(\frac{\eta}{\xi}\right)^2}} + \frac{\gamma^2}{\eta^2} \right\} - \frac{k'^2}{2} \ell n \frac{2\xi}{\gamma} - \frac{k'^2}{12} \frac{\gamma^2}{\eta^2} + k'^2 S(\zeta) \right] \tag{A-5}$$

in which $\zeta = k'\xi$,

and $$S(\zeta) = \frac{\zeta^2}{4|2} - \frac{\zeta^4}{6|4} + \frac{\zeta^6}{8|6} \cdots \tag{A-6}$$

For $\eta \geqslant 0$, the significant terms are like

$$k'^2 \ln \xi + \frac{k'^4 \xi^2}{16} \cdots$$

and there is no obvious reason why an asymptotic behavior occurs. This should receive more detailed study.